RFID-Micro Strain Gauge Sensor Analysis for Monitoring Bone Fracture Healing

Nicholas Hortance
School of Mechanical and Aerospace Engineering
University of Miami
Miami, FL
nmh23@miami.edu

Rafael Marques Braga
School of Electrical and Computer Engineering
University of Miami
Miami, FL
rxm403@miami.edu

***Abstract*—This paper provides a new design of a bio Nano strain gauge sensor to monitor the healing process of bone fracturing. The gauge sensor consists of capacitors and inductors and the information is read and interpreted through a RFID source. The paper contains studies on how the sensor was designed, its structure and its materials used with simulations of each design and a range of materials.**

***Index Terms*— Sensors, RFID (Radio frequency identification), Bone fracturing, Strain gauge sensor, Internal Fixation. LD1, LD2, Micro1, Micro2** *(key words)*

I. Introduction

Biocompatible sensors are capable of revolutionizing current therapeutic treatments due to their ability to progressively monitor the treatments response. Such sensors are able to provide live information on a species' behavior and status such as glucose levels, body temperature and blood pressure. Furthermore, they are able to give individualized and accurate status for potentially a wide-range of issues.

One such issue these sensors could be applied to is the treatment of broken bones. One of the current treatments for femur bone fractures is osteosynthesis [1-3], a procedure that uses internal fixation, wherein the broken bones are held in place by metal plates and screws that apply an external load, allowing the severed bone ends to conjoin. After the procedure is performed, the patient must return to the hospital repeatedly so that x-ray scans can be obtained to track the healing process. Currently, there exist few attempts at providing real-time, continuous data collection of the healing process for a once fractured bone. One particular research group developed an RFID (radio frequency identification) strain gauge sensor for this type of monitoring [4]. This method intuitively monitors the healing process by correlating the external load from the plates to the strain of the sensor. However, their sensor was relatively large (a few mm in size) and could be improved in terms of their performance throughout the healing process.

Thus, a smaller strain-gauge sensor could make implantation into the body more manageable and monitoring of the bone healing process more accurate. In this project, COMSOL software was utilized to simulate the performance of different strain-gauge sensors under different loading conditions and compare them to designs in literature [5].

II. Related Work

RFIDs, or Radio frequency identification devices, are tags, which can be either active or passive, that function using electromagnetic fields to identify objects or track tags which contain electronically stored information. These RFIDs can be found in every industry from clothing and cash to be implanted in animals and people. Active RFIDs use battery powered tags, these are able to emit its own signal. However, the passive RFIDs do not require any internal battery and these work by having a RFID reader with transmits electromagnetic waves as energy, which is then received and used by the tag and its integrated circuit delivering a signal back to the radio frequency reader [11]. Using a sensor which uses RFID technology transmitting a different frequency as the sensor's data is changed can be implemented on this study as a passive RFID can be implemented on the human body and be used to transmit data without the need of any wires or bulky devices.

A gauge sensor is a circuit which usually converts an external force, pressure, stress or strain to resistance. This resistance will vary depending on the force exerted to the device and the properties of the designed sensor [11]. A gauge sensor can be used combined with the RFID technology to monitor the healing process of a bone fracture without the need of any other large device except for the RFID reader which can be operated wirelessly.

Regularly, for a gauge sensor to be implemented to a RFID a complex integrated circuit is required. These usually contain a sensing black, a supply block, the RFID microchip and pin diodes for the antenna for it to be able to transmit a signal [11]. Inside these other ICs can be found such as a Wheatstone bridge for the gauge sensor in the sensing block to change a force implemented in the sensor to a different resistance accordingly. Op-amps and other circuits must also be implemented to change the resistance to frequency and therefore have a different signal transmitted by the tag. This makes the design of the sensor too complex for it to be made in such as a small scale and to be implantable in animals or humans to aid in the bone fracture healing process. This requires a new design of a sensor to be developed so it can have more advanced bio medical applications.

III. Proposed Work

As it can be seen in studies made, a stretchable RFID used for wireless strain sensing was proposed by using a LC circuit [5]. In the circuit, as a external force acts on the circuit, its capacitance is changed, impacting the resonant frequency which is read by the RFID reader. However, this study was done using non-bio compatible materials and in millimeter scale. A further study will be made on how this design can be tweaked and implemented in a biomedical application such as the bone healing. A continuation of the study will be made with different materials to analyze which bio-compatible material can be best used as a gauge sensor and continue with the same resonant frequency range. Another specification of the design is which its dimension should be decreased, and its RFID function enhanced.

To complete this research, studies will be made using COMSOL Multiphysics. A force study should be made to see how different forces applied to the sensor impacts its displacement. This displacement will therefore change the capacitance of the circuit and its resonant frequency. The resonant frequency study will also be made to determine the frequency which shall be used by the RFID reader. This reader will receive the data for it to continually analyze the movement and stress which the fracture bone undergoes in a certain period of time.

IV. Experimental Design

A. Structure

The RFID strain-gauge design implemented here consisted of a polymeric backing along with a conductive circuit (composed of a single turn inductor and an interdigitated capacitor). In developing the strain-gauge sensor circuit portion for this study, two designs found in literature were mimicked and designed in Creo Parametric software, and are referred to as LD1 and LD2 [5]. The remaining two circuit designs were similar to the literature designs in that their dimensions were scaled down 1:1000 and are referred to as Micro1 and Micro2 (Fig 1). The similarity in the designs allowed for direct comparison between them in the results.

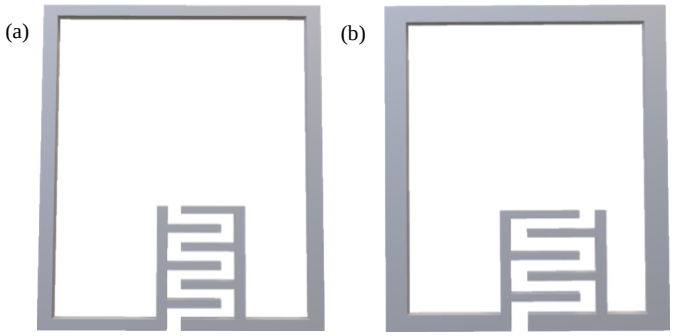

Fig 1. (a) LD1 and Micro1 circuit-portion of RFID strain-gauge design. (b.) LD2 and Micro2 circuit-portion of RFID strain-gauge design

B. Materials

Since the sensor is meant to be placed inside the body, the materials that are used must satisfy a biocompatibility condition. Polyurethane and polyimide are both proven biocompatible polymeric materials, so they were both used in evaluating the performance of the different sensor designs [6, 7]. Polyimide was also chosen because of its previously documented use in commercially available Nano-strain gauges. As well, copper is a well-known material that has a high conductivity, low cytotoxicity, and has also served as an antibacterial surface [8, 9]. It is for these reasons that copper was also chosen as a material for the circuit portion of the design. Lastly, single walled carbon nanotubes (SWCNT) were also used as a material for the circuit portion because of its low resistivity and high young's modulus. SWCNT biocompatibility is still under debate, however there are several sources that confirm the notion that they are biocompatible which is why they were included in the project [10].

C. Simulations

The simulations that were chosen to characterize the different combinations of materials and designs were based on a structural analysis. Namely, a variable force-controlled loading condition, variable strain-controlled loading condition, and an Eigen frequency analysis were performed. The force-controlled loading condition involved loads placed on the edge of the polymer material in the range of 1 to 50N with an increment of 1 N for the aforementioned literature designs, LD1, and LD2, whereas a load range of 1mN to 50mN with an increment of 1 mN was used for the scaled designs (Micro1 and Micro 2). Similarly, strain-controlled loading was applied on the edge of the polymer with a strain range of 1 to 4 % of the polymers width for both LD1 and LD2 and Micro1 and Micro2 respectively. The chosen range for the strain loading was selected for direct comparison to the final results found in literature [5]. Lastly, an Eigen-Frequency study was performed, with a focus on the sensor's 3rd harmonic, by loading the LD designs with 50 N and the Micro designs with 50mN. This study was conducted in order to identify possible issues in the integrity of the sensor.

D. Calculations

The following equations [5] were implemented in a MATLAB script to find the fundamental frequency (F) for the different material-design combinations:

$$L = 4\begin{Bmatrix} l_b \ln\left(\frac{2A}{a(l_b+l_c)}\right) + l_a \ln\left(\frac{2A}{a(l_b+l_c)}\right) \\ +2[a + l_c - (l_a + l_b))] \end{Bmatrix}^{nH} \quad (1)$$

$$C = \epsilon_0 \epsilon_r t\left(l_f - d\right)\left(\frac{2n-1}{g}\right) + nC_p(F) \quad (2)$$

$$l_c = \sqrt{l_b^2 + l_a^2} \quad (3)$$

$$F = \frac{1}{2\pi}\sqrt{\frac{1}{LC} - \left(\frac{R}{L}\right)^2} \quad (4)$$

The fundamental frequency, as seen in equation 3, is related to the inductance of the one turn inductor, the capacitance (C), and the resistance of the inductor (R). The dimensions related to the inductor and capacitor were used in evaluating the

inductance and resistance values, in which l_b and l_a were the inductor outer width and outer width respectively, l_c was the distance between diagonal corners of the inductor, 2a was the turn width of the inductor, A was the outer area of the inductor, n was the number of fingers used in the capacitor, d was the gap between a finger to the main bar, g was the gap between two adjacent fingers, ϵ_0 and ϵ_r were the vacuum and relative permittivity, and t was the thickness of the circuit. Lastly, the faradaic capacitance, C_p, was included in equation (2) to account for the inductors innate capacitance.

In performing the calculations as well as the simulations certain assumptions were held. One of which was that the material properties did not change due as a result of the loading condition, essentially meaning that the material properties were constant. As well, the faradaic capacitance was assumed to be 5 x 10^{-12}F because this value is not easily obtained nor is readily available in literature.

V. Results and Discussion

As mentioned previously, the first simulation that was performed was the variable force-controlled loading. This simulation yielded a visible response of the total displacement of the sensor, a representative image shown in Fig 2 (LD1 with copper and polyimide).

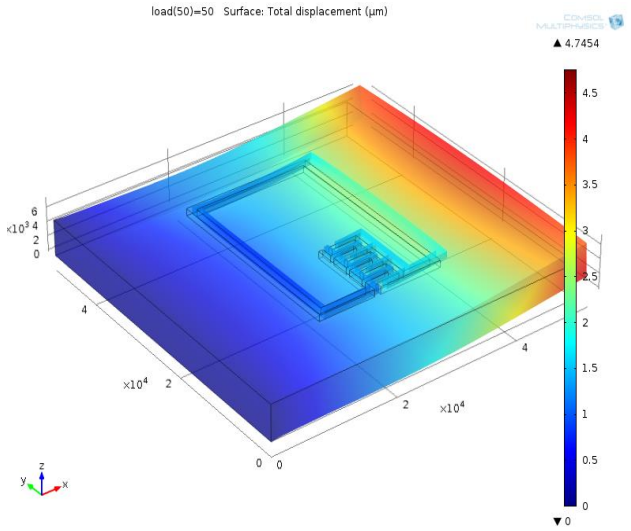

Fig 2. Total displacement (μm) for the LD1 design using a copper circuit and polyimide backing

Fig 2 shows that the maximum displacement occurred on the surface where the load was originally placed. The following figures yielded x-displacement values obtained for LD1 and LD2 under the four different material combinations.

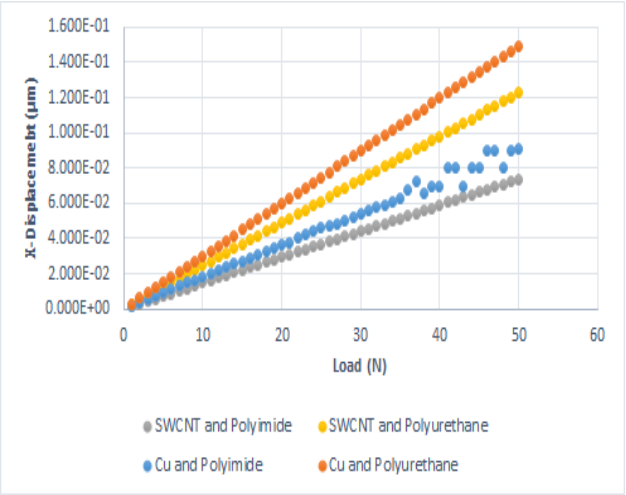

Fig 3. X-displacement (μm) from force loading for LD1 comparing copper and swcnt for the circuit, and polyimide and polyurethane for the backing

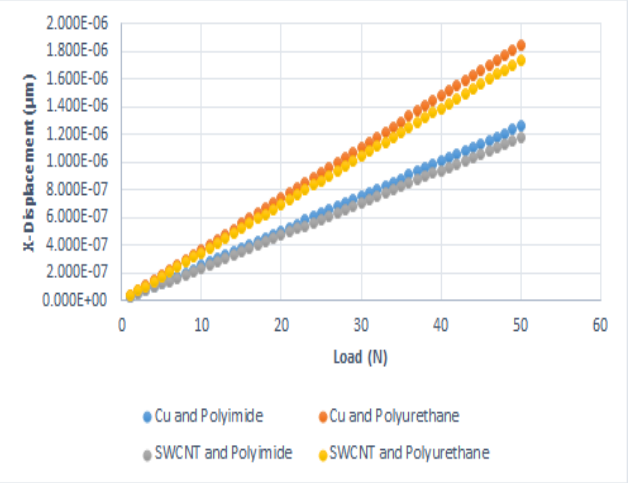

Fig 4. X-displacement (μm) from force loading for LD2 comparing copper and swcnt for the circuit, and polyimide and polyurethane for the backing

It was seen from Fig 3 and Fig 4 that the susceptibility of the sensors decreased as materials were changed from polyurethane to polyimide, and from copper to single walled carbon nanotubes. However, this trend was more apparent in the LD1 design compared to LD2, where LD2's circuit material played a lesser role compared to that of the polymer backing (Fig 4). Micro1 and Micro2 designs had almost identical displacement values (not shown here). It is also important to note that the displacement values are extremely small, and effectively inconsequential for monitoring the healing process of a fractured bone. Thus, the variable loading simulation was used only for qualitative analysis, and the subsequent strain loading simulation was conducted in order to give more substantial data.

The strain loading condition, in principle, is similar to the variable loading condition in that they both caused a displacement in the x-direction. However, by dictating the percentage of displacement relative to the polymer's original length, displacement values more representative of the healing process of a fractured bone was guaranteed. It

was seen that the combination of copper and polyurethane sensor materials was predominantly the set that had the highest sensing capability, in that they had the largest slope in the x-displacement vs strain curves (Fig 5, 6, and 7). A larger slope essentially meant that for the same strain, a higher capacitance value would be obtained. Only the Micro2 design illustrated that SWCNT and polyurethane materials yielded a larger slope than copper and polyurethane materials.

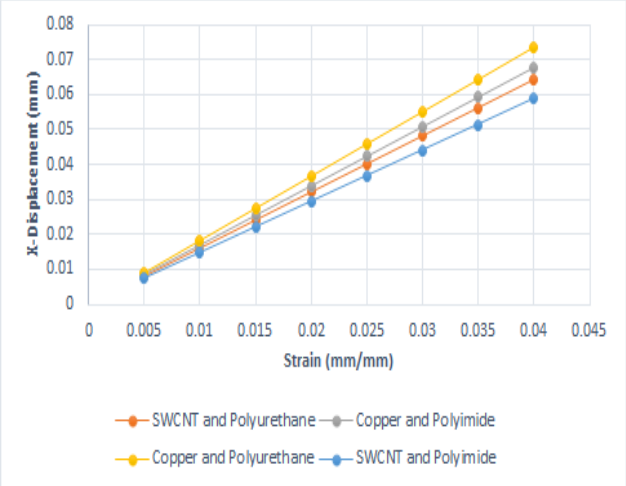

Fig 5. X-displacement (mm) from strain loading for LD1 comparing copper and swcnt for the circuit, and polyimide and polyurethane for the backing

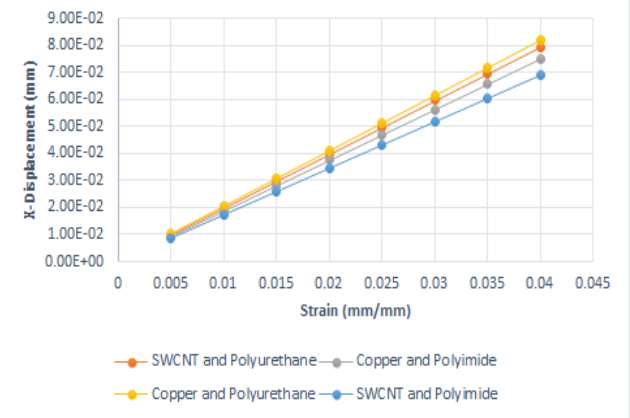

Fig 6. X-displacement (µm) from strain loading for LD2 comparing copper and swcnt for the circuit, and polyimide and polyurethane for the backing

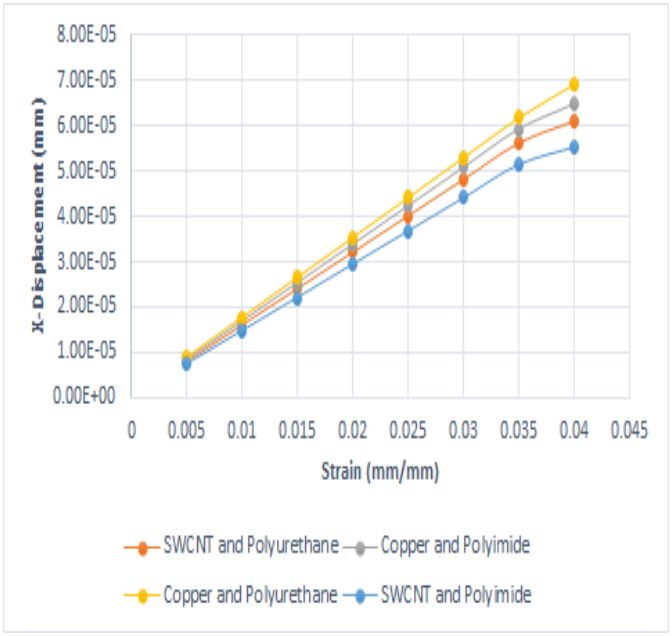

Fig 7. X-displacement (µm) from strain loading for Micro1 comparing copper and swcnt for the circuit, and polyimide and polyurethane for the backing

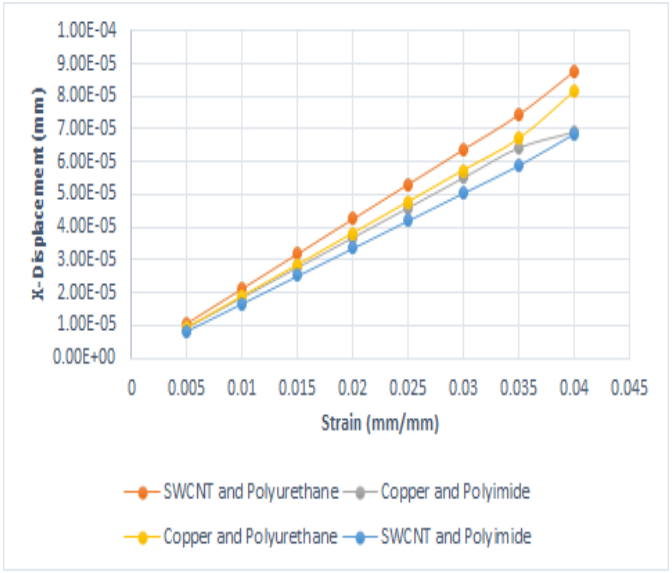

Fig 8. X-displacement (µm) from strain loading for Micro2 comparing copper and swcnt for the circuit, and polyimide and polyurethane for the backing

It can also be seen from figures 5 through 8 that the differences in x-axis displacement between the different combinations of materials increases as the strain increases. This is seen in that at a low strain of 0.5% all of the combinations of materials have almost identical displacement values, but this does not hold true at a strain of 4%.

Additionally, in comparing the LD and Micro designs, it was seen that the Micro design's x-axis displacements were approximately a thousandth of the LD designs. This essentially meant that scaling the LD designs was met with an equally proportional decrease in the displacement.

The last simulation that was performed was an Eigen-frequency study. The representative image showing the surface

displacement field is illustrated in Fig 9. The third Eigen-frequency was chosen as a basis for comparison because it was seen to have the maximum x-displacement inside of the capacitor. Figure 10 shows the resulting x-displacements for all four designs (LD1, LD2, Micro1, Micro2) all with a polyimide backing and comparing single walled carbon nanotube to copper circuit material. First, it was seen that the materials used for the circuit and polymer backing yielded the same Eigen-frequency for each respective design, which is why SWCNT and polyimide as well as copper and polyimide are grouped together in double bar graph. As well, in comparing the LD and Micro designs, the Micro designs appeared to have Eigen-frequencies a thousandth of the LD designs'. This increase in the Eigen-frequencies could pose an issue during the use of the sensor, since it could be more susceptible to breaking once implanted in the body.

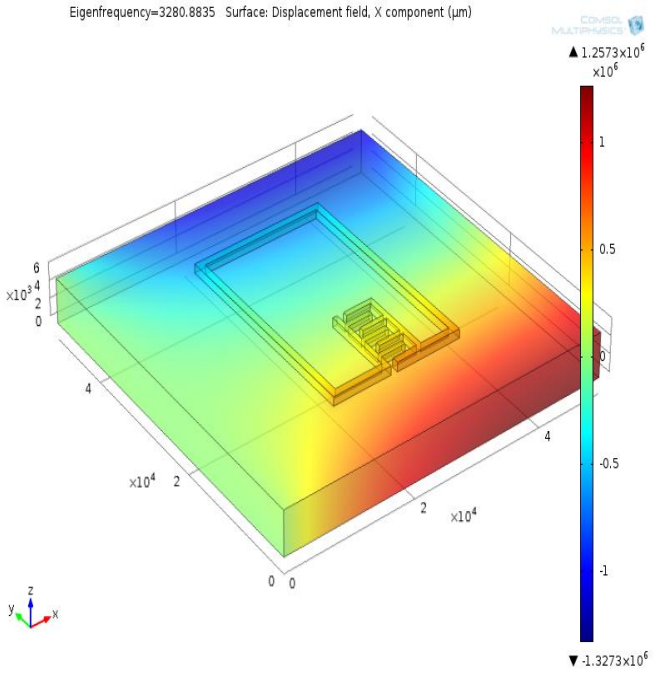

Fig 9. Total displacement (µm) for the LD1 design using a copper circuit and polyimide backing at its 3rd Eigen frequency

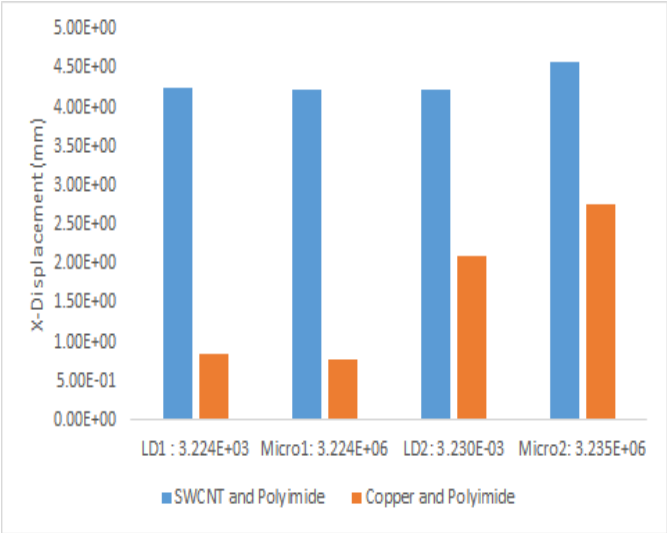

Fig 10. Bar Plot of the x-displacement (mm) at its 3rd Eigen frequency for the LD and Micro design comparing copper and swcnt for the circuit and using polyimide for the backing

Furthermore, Fig 10 shows that copper and polyimide materials had lower displacements as a result of the loading compared to the SWCNT and polyimide material combination. Results for polyurethane were not obtained due to lack of time.

After performing these simulations, final calculations of the capacitance, inductance and resistance values were made in order to obtain the (electrical) natural frequency values shown in figures 11 to 14.

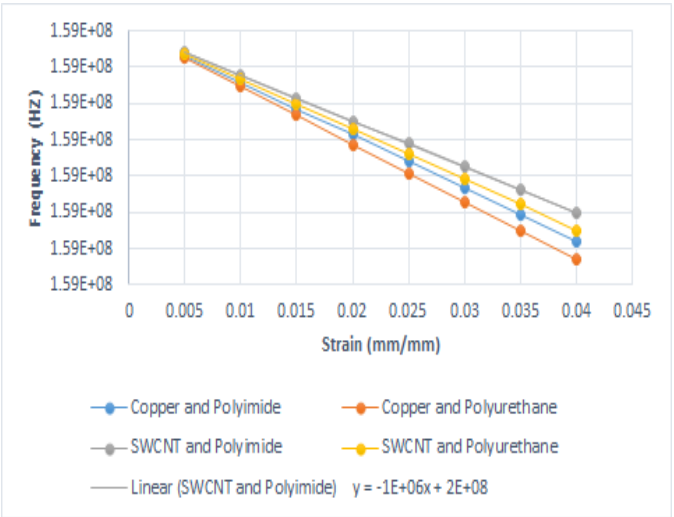

Fig 11. Frequency (Hz) as a result of strain loading for LD1 comparing copper and swcnt for the circuit, and polyimide and polyurethane for the backing

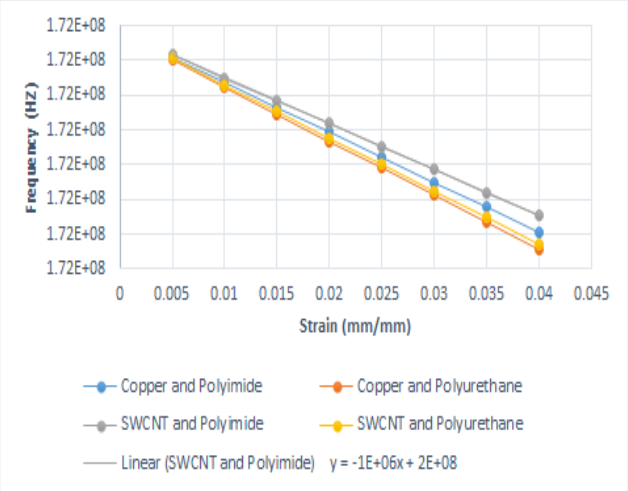

Fig 12. Frequency (Hz) as a result of strain loading for LD2 comparing copper and swcnt for the circuit, and polyimide and polyurethane for the backing

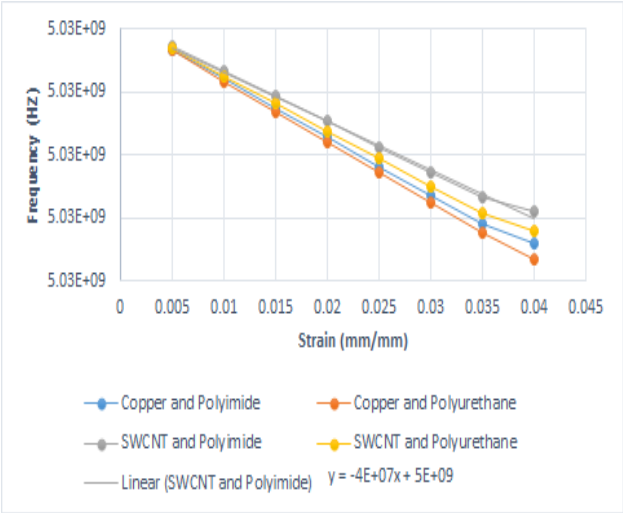

Fig 13. Frequency (Hz) as a result of strain loading for Micro1 comparing copper and swcnt for the circuit, and polyimide and polyurethane for the backing

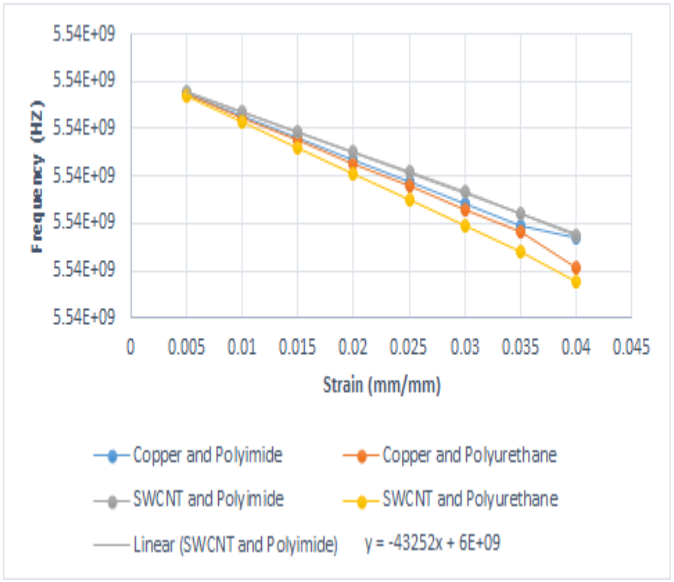

Fig 14. Frequency (Hz) as a result of strain loading for Micro2 comparing copper and swcnt for the circuit, and polyimide and polyurethane for the backing

Figures 11 to 13 show that the combination of materials that had the highest slope, just as in the strain-controlled loading study, was copper and polyurethane. These figures correspond to LD1, LD2, and Micro1 structural designs. In this case, the highest slope corresponded to higher sensing because as the strain increases the frequency changes by a larger amount compared to the other designs. However, similar to the strain-controlled loading study, Micro2 (Fig 14) was the only design that had its highest slope using SWCNT and polyurethane. The frequency values obtained for the LD designs were comparable in magnitude to that found in literature [5], and any discrepancies between the values can be attributed to the different material that was used for the circuit as well as the difference in thickness of the electrode. Comparison of the frequency values obtained in this project to that found in literature is beneficial as it affirms the validity of the Micro designs. It is also important to note that the LD and Micro designs differ by a little over one magnitude. This means that scaling the LD designs by a thousandth resulted in an increase in natural frequency equivalent to one magnitude. Lastly, Fig 11 and 12 shows that a frequency difference of about 1e7 Hz exists between the LD1 and LD2 design, whereas a difference of about 5e8 Hz exist between the Micro1 and Micro 2 designs. This essentially means that at a smaller scale, the change in dimensions of the circuit plays a greater role in the natural frequency of the sensor. Thus, the designer should have greater control over which frequencies will be passed by the sensor by simply changing the dimensions of the circuit a few micrometers.

VI. Conclusion

RFID strain-gauge sensors are powerful tools that can potentially render continuous monitoring of a fractured bone's healing process. However, scaled-down versions of these sensors are capable of increasing sensitivity as well as increase

comfort for the user. Through the studies performed in this project, it was seen that a micron scaled sensor, Micro 2, developed using single walled carbon nanotubes and polyurethane can match the level of sensitivity as those found in literature. Furthermore, the Micro2 design showed to have a higher resonant frequency when compared to the other designs making it a better RFID sensor working in the ultra-high frequency range allowing a long-read range of about 5-6 meters due to its long wavelength. The Micro2 design also showed to have a higher displacement vs strain slope when compared to the Micro1 design making the Micro2 a better gauge sensor since that brings a higher capacitance change. It also provided the smaller size against the LD2 design, while providing the same displacement to size and force ratio, this gives the best possible flexibility and a even higher displacement with the right choice of materials.

In order to improve/characterize this design, further experimental studies on vibrations inside of the body would have to be performed to know the body's influence on the sensor. As well, a magnetic resonance study would help to evaluate the gauge factor of the sensor which is an important metric in characterizing a strain-gauge sensor.

REFERENCES

[1] M. Mageed, T. Steinberg, N. Drumm, N. Stubbs, J. Wegert, and M. Koene, "Internal fixation of proximal fractures of the 2nd and 4th metacarpal and metatarsal bones using bioabsorbable screws," *Australian veterinary journal*, vol. 96, no. 3, pp. 76-81, 2018.

[2] B. Schaller, J. P. M. Burkhard, M. Chagnon, S. Beck, T. Imwinkelried, and M. Assad, "Fracture Healing and Bone Remodeling With Human Standard-Sized Magnesium Versus Polylactide–Co-Glycolide Plate and Screw Systems Using a Mini-Swine Craniomaxillofacial Osteotomy Fixation Model," *Journal of Oral and Maxillofacial Surgery*, 2018.

[3] M. Bottlang, S. M. Madey, K. Wirtz, and S. Tsai, "FLEXIBLE PLATE FIXATION OF BONE FRACTURES," ed: US Patent App. 15/712,967, 2018.

[4] C. Moß, N. Weinrich, K. Seide, and J. Müller, "Wireless recording system for long-term monitoring of bone fracture healing," in *World Congress on Medical Physics and Biomedical Engineering, September 7-12, 2009, Munich, Germany*, 2009, pp. 446-448: Springer.

[5] J. Kim, Z. Wang, and W. S. Kim, "Stretchable RFID for wireless strain sensing with silver nano ink," *IEEE Sensors Journal*, vol. 14, no. 12, pp. 4395-4401, 2014.

[6] R. Richardson Jr, J. Miller, and W. M. Reichert, "Polyimides as biomaterials: preliminary biocompatibility testing," *Biomaterials*, vol. 14, no. 8, pp. 627-635, 1993.

[7] M. J. Wiggins, M. MacEwan, J. M. Anderson, and A. Hiltner, "Effect of soft-segment chemistry on polyurethane biostability during in vitro fatigue loading," *Journal of Biomedical Materials Research Part A*, vol. 68, no. 4, pp. 668-683, 2004.

[8] B. Bagchi *et al.*, "Antimicrobial efficacy and biocompatibility study of copper nanoparticle adsorbed mullite aggregates," *Materials Science and Engineering: C*, vol. 32, no. 7, pp. 1897-1905, 2012.

[9] F. Heidenau *et al.*, "A novel antibacterial titania coating: metal ion toxicity and in vitro surface colonization," *J Mater Sci Mater Med*, vol. 16, no. 10, pp. 883-8, Oct 2005.

[10] L. P. Zanello, B. Zhao, H. Hu, and R. C. Haddon, "Bone cell proliferation on carbon nanotubes," *Nano letters*, vol. 6, no. 3, pp. 562-567, 2006.

[11] E. DiGiampaolo, A. DiCarlofelice and A. Gregori, "An RFID-Enabled Wireless Strain Gauge Sensor for Static and Dynamic Structural Monitoring," in IEEE Sensors Journal, vol. 17, no. 2, pp. 286-294, Jan.15, 15 2017